2008

Orbital magnetization of graphene and graphene nanoribbons

Junfeng Liu
Peking University

Zhongshui Ma
University of Wollongong, zma@uow.edu.au

Anthony Wright
University of Wollongong, arw75@uow.edu.au

Chao Zhang
University of Wollongong, czhang@uow.edu.au

Orbital magnetization of graphene and graphene nanoribbons

Junfeng Liu, Zhongshui Ma, A. R. Wright, and Chao Zhang

Citation: Journal of Applied Physics **103**, 103711 (2008); doi: 10.1063/1.2930875
View online: http://dx.doi.org/10.1063/1.2930875
View Table of Contents: http://scitation.aip.org/content/aip/journal/jap/103/10?ver=pdfcov
Published by the AIP Publishing

Orbital magnetization of graphene and graphene nanoribbons

Junfeng Liu,[1] Zhongshui Ma,[1,2] A. R. Wright,[2] and Chao Zhang[2,a)]
[1]*School of Physics, Peking University, Beijing 100871, People's Republic of China*
[2]*School of Engineering Physics, University of Wollongong, New South Wales 2552, Australia*

(Received 7 February 2008; accepted 28 March 2008; published online 22 May 2008)

We present a quantitative analysis on orbital magnetization of graphene under a magnetic field. The energy spectra were obtained by solving Harper equation for a honeycomb lattice. The effect of the next-nearest-neighbor hopping (NNNH) is to increase the period of the magnetic subbands in ϕ/ϕ_0 from 1 to 6 (where ϕ is the magnetic flux through a unit cell and ϕ_0 is the flux quanta). The shifts of the energy levels due to the NNNH vary with the magnetic field. The Holmholtz free energy at the points $\phi/\phi_0=6n+1$ is lowered as compared to that with the nearest neighbor hopping only. For graphene nanoribbons, the magnetic susceptibility is very sensitive to the ribbon width and chirality. The zero-field susceptibility increase with the ribbon width. © *2008 American Institute of Physics*. [DOI: 10.1063/1.2930875]

I. INTRODUCTION

The electronic properties of two-dimensional (2D) lattices under a uniform perpendicular magnetic field have been known to be dramatically changed by introducing a nonuniform part in the applied magnetic field.[1–7] For instance, for a square lattice, both the symmetry and the number of subbands in the energy spectrum are modified by introducing a field modulation. Besides, for the so-called T_3 lattice, which is a kind of non-Bravais lattice, not only the energy spectrum but also the localization property of an electronic state is significantly changed by the field modulation.

Recent progress in isolating single sheets of graphite[8–11] has sparked interest in graphene-based nanoelectronics. Experiments have already demonstrated anticipated physics, such as electron-hole symmetry and the half-integer quantum Hall effect,[9,10] the finite conductivity at zero charge-carrier concentration,[9] the strong suppression of weak localization,[12–15] etc. By further confining the electrons in the graphene plane, one can obtain one-dimensional structures which we refer to as graphene nanoribbons (GNRs). It has been suggested that these GNRs could be used as field-effect transistors.[16–18] These properties promise building blocks for the technological applications in molecular electronic and optoelectronic devices.

In graphene, the conduction and valance bands touch each other at isolated points in the Brillouin zone (K and K'). Undoped graphene is a gapless semiconductor, or a semimetal, with vanishing density of states at the Fermi level. Low-energy electronic states of graphene with a linear dispersion at the corner of the Brillouin zone are described by the "relativistic" massless Dirac equation. This relativistic kinematical description of graphene is confirmed in the quantum Hall studies[19] and gives us theoretical insight into exotic transport,[20] magnetic correlation,[21,22] and dielectric[23] properties observed in this material.

It is expected that the electrons in a honeycomb lattice can have very different thermodynamic properties, as compared to that of a free 2D electron gas. Under the nearest-neighbor hopping (NNH) approximation, the magnetic subband has a symmetrical butterfly pattern and the period is the flux quanta ϕ_0. When the next-NNH (NNNH) term is included, the period becomes $6\phi_0$. We shall show that this will lead to a profound change in the thermodynamic properties of graphene. For the strength of NNNH around 10% of that of the NNH, the free energy at the points $\phi/\phi_0=6n+1$ is lower. Our results suggests that while the NNNH term correction in the single electronic properties may be small, it leads to a much greater effect on the thermodynamic properties of a graphene. For GNRs, the magnetic susceptibility is very sensitive to the ribbon width and orientation. The zero-field orbital magnetic susceptibility increases with the ribbon width. The susceptibility for the zigzag width is round 50% stronger than that of the armchair ribbon.

The paper is organized as follows. In Sec. II, we introduce the model and discuss the basic processes of calculations. The energy spectrum of a graphene as a function of the magnetic flux is given. We then extend the discussion to the transverse finite graphene and show the magnetic subband structure for a ribbon. We explicitly compute orbital magnetizations of graphene and ribbon. Our numerical results are given in Sec. III. Finally, we summarize our results in Sec. IV.

II. ELECTRONIC PROPERTIES OF GRAPHENE UNDER A MAGNETIC FIELD

A unit cell, whose wave vectors are given by $\mathbf{a}_1=\sqrt{3}a(\sqrt{3}/2,1/2)$ and $\mathbf{a}_2=\sqrt{3}a(\sqrt{3}/2,-1/2)$ in a honeycomb lattice contains two atoms denoted as A and B, where a is the C–C bond length. The tight-binding electron spectrum of a 2D honeycomb lattice under a magnetic field can be obtained by solving the following Schrödinger equation:

$$E\psi_i=\sum_{j,k}(te^{i\gamma_{ij}}\psi_j+t'e^{i\gamma_{ik}}\psi_k), \tag{1}$$

where t is the NNH integral between i and j, t' is the NNH integral between i and k, and $\gamma_{ij}=(2\pi/\phi_0)\int_i^j\mathbf{A}\cdot d\mathbf{l}$ is the magnetic phase factor, with $\phi_0=hc/e$ being the magnetic flux quantum. The eigenvalue problem can be written as

a)Electronic mail: czhang@uow.edu.au.

$$E\psi_B(x,y) = t\left[\psi_A(x-a,y) + \sum_{s=\pm}\psi_A\left(x+\frac{a}{2}, y+s\frac{\sqrt{3}a}{2}\right)e^{is2\pi/3f(x/a+1/4)}\right] + t'\sum_{s=\pm}\left[\sum_{s'=\pm}\psi_B\left(x+s'\frac{3a}{2}, y+s\frac{\sqrt{3}a}{2}\right)e^{is2\pi/3f(x/a+s'3/4)}\right.$$
$$\left. + \psi_B(x,y+s\sqrt{3}a)e^{is4\pi/3fx/a}\right], \tag{2}$$

where $f=\phi/\phi_0=3\sqrt{3}Ba^2/(2\phi_0)$ is the magnetic flux through the hexagon in units of ϕ_0. ψ_A and ψ_B are the wave functions of sublattices A and B. Because we choose the system as infinite in the y direction, we then assume plane wave behavior in the y direction

$$\begin{bmatrix}\psi_A(x,y)\\ \psi_B(x,y)\end{bmatrix} = \begin{bmatrix}\psi_A(x)\\ \psi_B(x)\end{bmatrix}e^{ik_y y}. \tag{3}$$

Equation (2) can be simplified as

$$E\psi_B(x) = t\left\{\psi_A(x-a) + 2\psi_A\left(x+\frac{a}{2}\right)\cos\left[\frac{2\pi}{3}f\left(\frac{x}{a}+\frac{1}{4}\right)+\frac{\sqrt{3}a}{2}k_y\right]\right\} + 2t'\left\{\psi_B(x)\cos\left[\frac{4\pi}{3}f\left(\frac{x}{a}\right)+\sqrt{3}ak_y\right]\right.$$
$$\left. + \sum_{s=\pm}2\psi_B\left(x+s\frac{3a}{2}\right)\cos\left[\frac{2\pi}{3}f\left(\frac{x}{a}+s\frac{3}{4}\right)+\frac{\sqrt{3}a}{2}k_y\right]\right\}. \tag{4}$$

By setting $\psi_{Bm}=\psi_B(x)$ at $x=(3a/2)m$ and $\psi_{Am}=\psi_A(x)$ at $x=(3a/2)m+a/2$, the above equation reads

$$E\psi_{Bm} = t\left\{\psi_{Am-1} + 2\psi_{Am}\cos\left[\pi f\left(m+\frac{1}{6}\right)+\kappa\right]\right\} + 2t'\left\{\psi_{Bm}\cos[2\pi fm+2\kappa] + \sum_{s=\pm}\psi_{Bm+s1}\cos\left[\pi f\left(m+s\frac{1}{2}\right)+\kappa\right]\right\}, \tag{5}$$

where $\kappa=(\sqrt{3}a/2)k_y$. Similar for A sites, we have

$$E\psi_{Am} = t\left\{\psi_{Bm+1} + 2\psi_{Bm}\cos\left[\pi f\left(m+\frac{1}{6}\right)+\kappa\right]\right\} + 2t'\left\{\psi_{Am}\cos\left[2\pi f\left(m+\frac{1}{3}\right)+2\kappa\right]\right.$$
$$\left. + \sum_{s=\pm}\psi_{Am+s1}\cos\left[\pi f\left(m+\frac{1}{3}+s\frac{1}{2}\right)+\kappa\right]\right\}. \tag{6}$$

These two equations can be written in a matrix form

$$E\psi_m = A_{m-1}^T\psi_{m-1} + C_m\psi_m + A_m\psi_{m+1}, \tag{7}$$

where

$$\psi_m = \begin{pmatrix}\psi_{Am}\\ \psi_{Bm}\end{pmatrix},$$

$$C_m = \begin{Bmatrix} 2t'\cos\left[2\pi f\left(m+\frac{1}{3}\right)+2\kappa\right] & 2t\cos\left[\pi f\left(m+\frac{1}{6}\right)+\kappa\right] \\ 2t\cos\left[\pi f\left(m+\frac{1}{6}\right)+\kappa\right] & 2t'\cos[2\pi fm+2\kappa]\end{Bmatrix}, \tag{8}$$

$$A_m = \begin{Bmatrix} 2t'\cos\left[\pi f\left(m+\frac{5}{6}\right)+\kappa\right] & t \\ 0 & 2t'\cos\left[\pi f\left(m+\frac{1}{2}\right)+\kappa\right]\end{Bmatrix}.$$

Equation (7) is the Harper equation for a graphene with next-nearest-neighbor coupling. For a rational flux $f=p/q$ with mutual primes p and q, Eq. (7) leads to the Bloch condition along the x direction

$$\psi_{m+N_x} = e^{iN_x\eta}\psi_m, \tag{9}$$

$$\begin{pmatrix} C_1 & A_1 & 0 & \cdots & A_0^T e^{-iN_x\eta} \\ A_1^T & C_2 & A_2 & \cdots & 0 \\ 0 & A_2^T & C_3 & \cdots & 0 \\ \cdots & \cdots & \cdots & \cdots & \cdots \\ A_0 e^{iN_x\eta} & 0 & 0 & \cdots & C_{N_x} \end{pmatrix}. \tag{10}$$

By diagonalizing the matrix, we can obtain $2q$ energy eigenvalues for a given $\mathbf{k}=(k_x,k_y)$. However, when q is sufficiently large, the butterfly spectrum is the same to all of the $\mathbf{k}$.

For graphene ribbons, the magnetic subband structure can be obtained in terms of the Harper equation [Eq. (7)] by imposing open boundary condition instead of the Bloch condition [Eq. (9)]. If the width of the ribbon is W (W is an integer), the open boundary condition reads

$$\psi_0 = \psi_{W+1} = 0. \tag{11}$$

Moreover, for armchair ribbons, the Harper equation [Eq. (7)] must be rewritten to include the translational symmetry along the armchair axis

$$E\psi_m = t'\psi_{m-2} + B_{m-1}\psi_{m-1} + D_m\psi_m + B_m\psi_{m+1} + t'\psi_{m+2}, \tag{12}$$

where

$$B_m = \begin{Bmatrix} 2t'\cos\left[\pi f\left(m+\frac{1}{2}\right)+3\kappa\right] & te^{i[\pi/3f(m+1/2)+\kappa]} \\ te^{-i[\pi/3f(m+1/2)+\kappa]} & 2t'\cos\left[\pi f\left(m+\frac{1}{2}\right)+3\kappa\right] \end{Bmatrix},$$

$$D_m = \begin{bmatrix} 0 & te^{-i(2/3\pi fm+2\kappa)} \\ te^{i(2/3\pi fm+2\kappa)} & 0 \end{bmatrix}. \tag{13}$$

The widths of the zigzag and armchair ribbons are defined in the same way as in Ref. 24.

In Figs. 1 and 2, we show the energy spectrum of a graphene as a function of the dimensionless magnetic flux $f=p/q$ for $t'=0.1t$. Compared to the spectrum of Ref. 1, the NNNH causes a significant distortion to the magnetic subbands. The spectrum is no longer symmetric about $E=0$ and about $f=\phi/\phi_0=0.5$. The new magnetic period of the spectra in ϕ/ϕ_0 is 6. Within one period, the spectra are symmetric about $\phi/\phi_0=3$. The original energy level at $E=0$ shifts to a lower energy. It is known that in the absence of the applied magnetic field, the t' term in the Hamiltonian leads to a redshift $\delta E=t'[4\cos(3ak_x/2)\cos(\sqrt{3}ak_y/2)+4\cos^2(\sqrt{3}ak_y/2)-2]$. When a constant B field is applied, the redshift due to the t' term varies with the B field, results in a spectrum given in Fig. 2. The Hall plateau at $B=0$ is

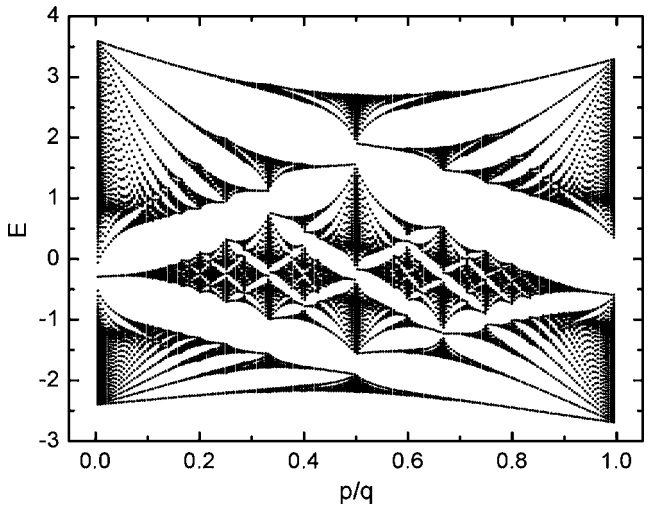

FIG. 1. Energy spectrum of graphene with next-nearest-neighbor coupling vs the applied magnetic field.

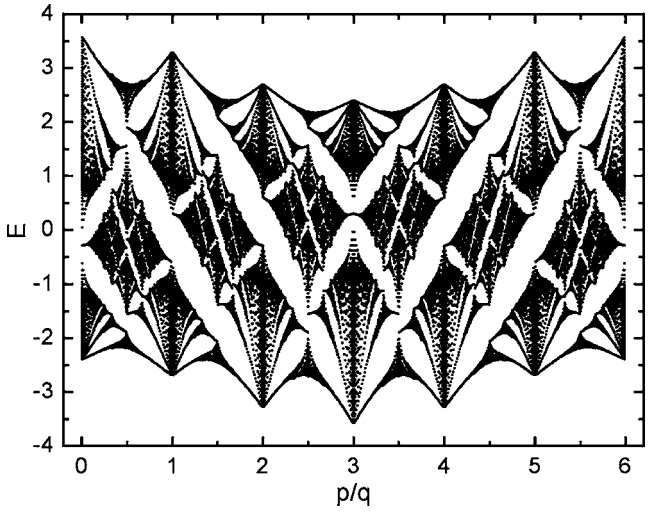

FIG. 2. Energy spectrum of graphene with next-nearest-neighbor coupling vs the applied magnetic field. A period is plotted.

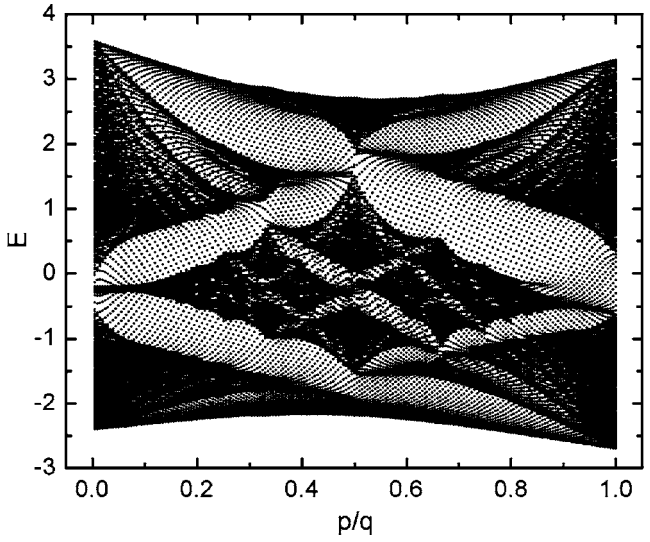

FIG. 3. Energy spectrum of a GNR with next-nearest-neighbor coupling vs the applied magnetic field.

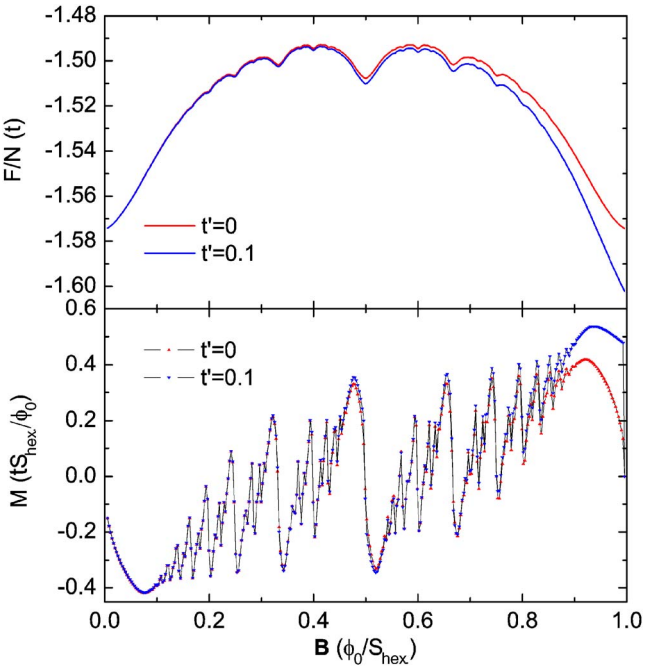

FIG. 4. (Color online) Upper panel: free energy as function of magnetic field at the room temperature $T=300$ K with and without next-nearest hopping. $q=701$. The number of electrons is fixed to half-filling $N=q$. Lower panel: the magnetization M as function of magnetic field.

now shifted to the negative energy side. The magnetic subband structure for a ribbon is shown in Fig. 3. For ribbons along the y direction, the wave-vector k_x is quantized by the boundary conditions. The ribbon boundaries lift the k_y degeneracy and lead to a finite dispersion. In this case, the original magnetic bandgaps for infinite graphene are now filled with different k_y levels. For a given k_y, one finds a set of levels in the gap. The dots in Fig. 3 represent those levels for several different values of k_y. If all k_y levels are plotted, the original gap will be filled completely when viewed in two dimensions. However, the system is not gapless. When viewed in three dimensions, one can see energy gaps whose positions vary with k_y.

III. ORBITAL MAGNETIZATION OF GRAPHENE

In this section, we will use the energy spectra of a graphene and a ribbon to calculate the orbital magnetization numerically. The magnetization can be obtained by the derivation of free energy with respect to the external magnetic field.

The Helmholtz free energy of the system is given as

$$F(B,T) = \mu N - k_B T \sum_s \ln(1 + e^{-\alpha-\beta\epsilon_s}). \tag{14}$$

Here, $\beta=(k_BT)^{-1}$ and $\alpha=\beta\mu$, the s summation is over these $2q$ energy eigenvalues. Because when q is sufficiently large, the butterfly spectrum almost the same to all the $\mathbf{k}$. In our calculation, we choose $q=701$ and ignore the summation over different $\mathbf{k}$.

The magnetic field dependent free energy is plotted in the upper panel of Fig. 4. For a 2D honeycomb lattice, there is no well-defined $1/B$, or the de Hass–van Alphen-type oscillation in the free energy because the gap of magnetic subband at given B is not constant. Under the nearest neighbor approximation, the free energy is symmetric about the $B=1/2$ point. The free energy has a local minimum at this point. Since the curve is periodic in ϕ/ϕ_0, the global minima of the free energy occur at $\phi=n\phi_0$, the thermodynamic equilibrium points. When the next nearest neighbor is included, the period of the free energy versus B field is 6, in this case, the free energy at original thermodynamic equilibrium points $\phi=\phi_0$ is lower than that for $t'=0$ by an amount $\Delta F/F \approx 2\%$.

The constant magnetic field induced orbit magnetic moment of the electron orbit. The magnetization per electron is defined as $M=-(1/N)(dF/dB)$. The M-B curves for both NNH and NNNH are shown in the lower panel of Fig. 4. The magnetization oscillates with the B field rapidly, reflecting the fast sweeping of the chemical potential through the magnetic subband. The system changes back and forth between the paramagnetic and diamagnetic phases. For the field strength of practical interest, the graphene is in the diamagnetic phase. The effect of the NNNH term is quite significant. It enhanced M by around 100% at the thermodynamic equilibrium point of $\phi=\phi_0$. In Fig. 5, we plot the susceptibility $\chi=-(1/N)(d^2F/dB^2)$ as a function of the magnetic field, the NNNH parameter is $t'=0.1t$. When the hopping parameters are fixed, the susceptibility oscillation decreases as the temperature increases.

For GNRs, the susceptibility is dependent strongly on the width and orientation of the ribbon. In the calculation of free energy of ribbons, the s summation in Eq. (14) should be over $2W$ energy eigenvalues and the wave vector in the transport direction of a ribbon with width of W. In Fig. 6, we show that the susceptibility with NNH is only for zigzag and armchair ribbons with various ribbon width. Moreover, the chemical potential is fixed to $\mu=0$. The edge states of the ribbon have a dominant effect on the low-field susceptibility. For both zigzag and armchair ribbons, the susceptibility increases rapidly as the ribbon width increases. This is mainly due to the fact that as the ribbon narrows, the edge states

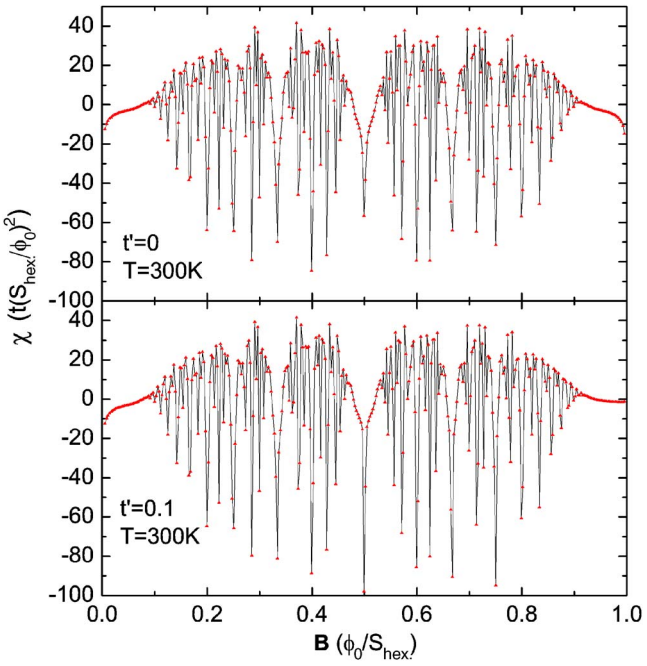

FIG. 5. (Color online) Susceptibility as function of magnetic field at the room temperature $T=300$ K. Top: only nearest neighbor hopping is considered. Bottom: the next-nearest hopping is considered with $t'=0.1$.

become more important. However, these edge states do not carry orbit magnetic moment at low field. For ribbons of same width, χ depends on the chirality of the ribbon. For ribbon width of 50, the zero-field susceptibility of the zigzag ribbon is around 20% stronger than that of the armchair ribbon. If the ribbon width is 20, this difference is more than 100%. As field intensity increases, the radius cyclotron orbit decreases and the edge states become less important. As a result, the difference in susceptibility of different ribbons disappears.

The temperature dependence of the susceptibility is shown in Fig. 7. The oscillatory magnetization leads to both positive and negative susceptibilities, depending on the value of the B field. The magnitude of χ decreases as temperature

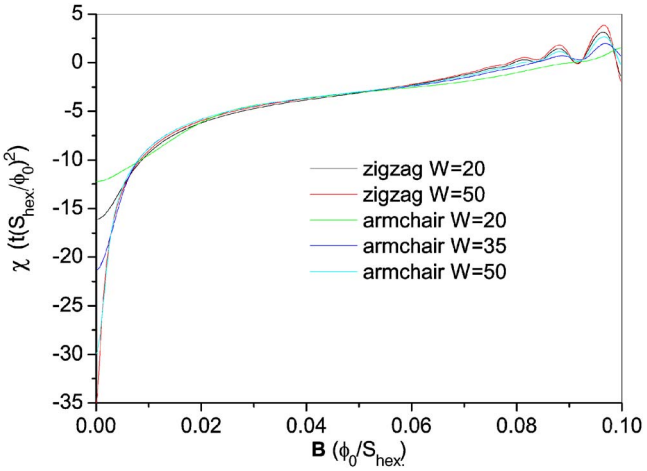

FIG. 6. (Color online) Susceptibility as function of magnetic field in the weak field region at the room temperature $T=300$ K for zigzag and armchair ribbons with various widths W. The chemical potential is fixed to $\mu=0$.

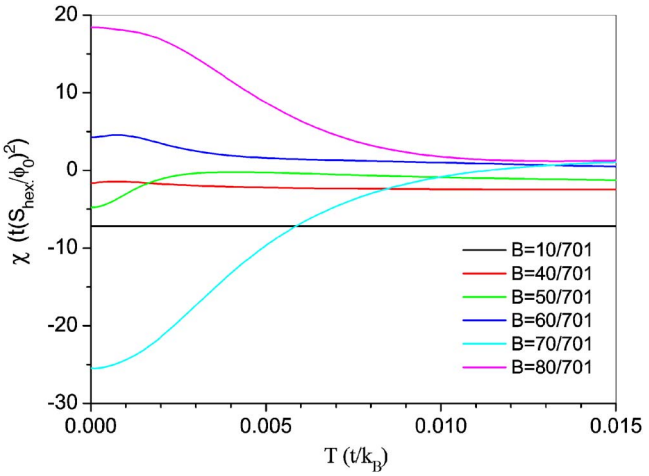

FIG. 7. (Color online) Susceptibility as function of the temperature, the room temperature 300 K is approximately at $T=0.01$. $N=q$, varied magnetic field strengths are considered.

increases. The temperature dependence around room temperature is close to the T^{-1} behavior. At a low field, χ is nearly temperature independent.

IV. SUMMARY

In summary, we have obtained a qualitative and quantitative results of the orbital magnetization in graphene and GNR. The magnetic field and temperature dependence of the magnetization and the magnetic susceptibility over a wide range of field and temperature range are presented at zero or finite temperatures, and at weak as well as strong magnetic fields. Our quantitative results indicate that the orbital magnetization is sensitive to the ribbon width and chirality, as well as the effect due the NNNH.

The result presented here should be useful in developing grapheme-based electronic and magnetoelectronic devices. Recently, there has been a great deal of renewed interest in magnetic properties of graphene-based structures.[20,21] Most recent studies concentrated on the spin magnetization. Application of graphene in magnetoelectronics involves controlling the local magnetization of graphene or GNRs. In general, the magnetization of graphene has contributions from the spin of the electrons and from their orbital motion. Our result on the orbital magnetization, together with the result on magnetization due to electron spins, provides useful information in selecting graphene structures with desired magnetic properties.

ACKNOWLEDGMENTS

C.Z. acknowledges the financial support from the Australian Research Council, J.F.L. and Z.S.M. acknowledge the financial support from the NNSFC Grant No.10674004 and NBRP-China Grant No. 2006CB921803.

[1]R. Rammal, J. Phys. (Paris) **46**, 1345 (1985).
[2]A. Barelli, J. Bellissard, and R. Rammal, J. Phys. (Paris) **51**, 2167 (1990).
[3]R. R. Gerhardts, D. Pfannkuche, and V. Gudmundsson, Phys. Rev. B **53**, 9591 (1996).
[4]A. Y. Rom, Phys. Rev. B **55**, 11025 (1997).
[5]Y. Iye, E. Kuramochi, M. Hara, A. Endo, and S. Katsumoto, Phys. Rev. B

70, 144524 (2004).
[6]M. C. Geisler, J. H. Smet, V. Umansky, K. von Klitzing, B. Naundorf, R. Ketzmerick, and H. Schweizer, Phys. Rev. Lett. **92**, 256801 (2004).
[7]G. Gumbs and C. Zhang, Solid State Commun. **115**, 163 (2000); R. R. Gerhardts and C. Zhang, Phys. Rev. Lett. **64**, 1473 (1990); C. Zhang, *ibid.* **65**, 2207 (1990).
[8]K. S. Novoselov, A. K. Geim, S. V. Morozov, D. Jiang, Y. Zhang, S. V. Dubonos, I. V. Grigorieva, and A. A. Firsov, Science **306**, 666 (2004).
[9]K. S. Novoselov, A. K. Geim, S. V. Morozov, D. Jiang, M. I. Katsnelson, I. V. Grigorieva, S. V. Dubonos, and A. A. Firsov, Nature (London) **438**, 197 (2005).
[10]Y. Zhang, Y. W. Tan, H. L. Stormer, and P. Kim, Nature (London) **438**, 201 (2005).
[11]C. Berger, Z. Song, X. Li, X. Wu, N. Brown, C. Naud, D. Mayou, T. Li, J. Hass, A. N. Marchenkov, E. H. Konrad, P. N. First, and W. A. de Heer, Science **312**, 1191 (2006).
[12]H. Suzuura and T. Ando, Phys. Rev. Lett. **89**, 266603 (2002).
[13]S. V. Morozov, K. S. Novoselov, M. I. Katsnelson, F. Schedin, L. A. Ponomarenko, D. Jiang, and A. K. Geim, Phys. Rev. Lett. **97**, 016801 (2006).
[14]D. V. Khveshchenko, Phys. Rev. Lett. **97**, 036802 (2006).
[15]E. McCann, K. Kechedzhi, V. I. Fal'ko, H. Suzuura, T. Ando, and B. L. Altshuler, Phys. Rev. Lett. **97**, 146805 (2006).
[16]B. Obradovic, R. Kotlyar, F. Heinz, P. Matagne, T. Rakshit, M. D. Giles, M. A. Stettler, and D. E. Nikoniv, Appl. Phys. Lett. **88**, 142102 (2006).
[17]Y. Ouyang, Y. Yoon, J. K. Fodor, and J. Guo, Appl. Phys. Lett. **89**, 203107 (2006).
[18]Q. Yan, B. Huang, J. Yu, F. Zheng, J. Zang, J. Wu, B.-L. Gu, F. Liu, and W. Duan, Nano Lett. **7**, 1469 (2007).
[19]Y. S. Zheng and T. Ando, Phys. Rev. B **65**, 245420 (2002).
[20]N. M. R. Peres, F. Guinea, and A. H. Castro Neto, Phys. Rev. B **73**, 125411 (2006); K. Ziegler, Phys. Rev. Lett. **97**, 266802 (2006); I. L. Aleiner and K. B. Efetov, *ibid.* **97**, 236801 (2006); A. Altland, *ibid.* **97**, 236802 (2006); P. M. Ostrovsky, I. V. Gornyi, and A. D. Mirlin, Phys. Rev. B **74**, 235443 (2006); K. Nomura and A. H. MacDonald, Phys. Rev. Lett. **98**, 076602 (2007).
[21]M. Fujita, K. Wakabayashi, K. Nakada, and K. Kusakabe, J. Phys. Soc. Jpn. **65**, 1920 (1996);; Y. Son, M. L. Cohen, and S. G. Louie, Nature (London) **444**, 347 (2006); L. Pisani, J. A. Chan, B. Montanari, and N. M. Harrison, Phys. Rev. B **75**, 064418 (2007); O. V. Yazyev and L. Helm, *ibid.* **75**, 125408 (2007).
[22]M. A. H. Vozmediano, M. P. Lopez-Sancho, T. Stauber, and F. Guinea, Phys. Rev. B **72**, 155121 (2005).
[23]E. H. Hwang, S. Adam, and S. Das Sarma, Phys. Rev. Lett. **98**, 186806 (2007); E. H. Hwang and S. Das Sarma, Phys. Rev. B **75**, 205418 (2007).
[24]K. Wakabayashi, M. Fujita, H. Ajiki, and M. Sigrist, Phys. Rev. B **59**, 8271 (1999).